



HAL
open science

**Cation-chloride cotransporters and the polarity of
GABA signaling 2 in mouse hippocampal parvalbumin
interneurons Running title: GABA signaling in
hippocampal parvalbumin interneurons**

Yo Otsu, Florian Donneger, Eric J Schwartz, Jean Christophe Poncer

► **To cite this version:**

Yo Otsu, Florian Donneger, Eric J Schwartz, Jean Christophe Poncer. Cation-chloride cotransporters and the polarity of GABA signaling 2 in mouse hippocampal parvalbumin interneurons Running title: GABA signaling in hippocampal parvalbumin interneurons. 2020. hal-02985908

HAL Id: hal-02985908

<https://hal.sorbonne-universite.fr/hal-02985908v1>

Preprint submitted on 2 Nov 2020

HAL is a multi-disciplinary open access archive for the deposit and dissemination of scientific research documents, whether they are published or not. The documents may come from teaching and research institutions in France or abroad, or from public or private research centers.

L'archive ouverte pluridisciplinaire **HAL**, est destinée au dépôt et à la diffusion de documents scientifiques de niveau recherche, publiés ou non, émanant des établissements d'enseignement et de recherche français ou étrangers, des laboratoires publics ou privés.

1

2

Cation-chloride cotransporters and the polarity of GABA signaling

3

in mouse hippocampal parvalbumin interneurons

4

5 Yo Otsu^{1,2,3,4}, Florian Donneger^{1,2,3}, Eric J Schwartz^{1,2,3} and Jean Christophe Poncer^{1,2,3*}

6

7 ¹ Inserm UMR-S 1270, 75005 Paris, France.; ² Sorbonne Université, F75005, Paris, France ;

8 ³ Institut du Fer à Moulin, F75005, Paris, France.

9 ⁴ Present address: Pain Management Research Institute, Kolling Institute of Medical Research,
10 Northern Clinical School, The University of Sydney and Royal North Shore Hospital, St.
11 Leonards, New South Wales, Australia

12

13 Running title: GABA signaling in hippocampal parvalbumin interneurons

14 Keywords: synaptic transmission, GABA, KCC2, chloride, transporters, hippocampus

15 Category: Research paper

16

17 * Correspondence should be addressed to Jean Christophe Poncer:

18 INSERM UMR-S 1270

19 17 rue du Fer à Moulin

20 75005 Paris, France

21 Tel. +33 1 45 87 61 18

22 E-mail : jean-christophe.poncer@inserm.fr

23 Key point summary

- 24 • Cation-chloride cotransporters (CCCs) play a critical role in controlling the efficacy and
25 polarity of GABAA receptor (GABAAR)-mediated transmission in the brain, yet their
26 expression and function in GABAergic interneurons has been overlooked.
- 27 • We compared the polarity of GABA signaling and the function of CCCs in mouse
28 hippocampal pyramidal neurons and parvalbumin-expressing interneurons.
- 29 • Under resting conditions, GABAAR activation was mostly depolarizing and yet
30 inhibitory in both cell types. KCC2 blockade further depolarized the reversal potential
31 of GABAAR-mediated currents often above action potential threshold.
- 32 • However, during repetitive GABAAR activation, the postsynaptic response declined
33 independently of the ion flux direction or KCC2 function, suggesting intracellular
34 chloride buildup is not responsible for this form of plasticity.
- 35 • Our data demonstrate similar mechanisms of chloride regulation in mouse
36 hippocampal pyramidal neurons and parvalbumin interneurons.

37

38 **Abstract**

39 Transmembrane chloride gradients govern the efficacy and polarity of GABA signaling in
40 neurons and are usually maintained by the activity of cation chloride cotransporters, such as
41 KCC2 and NKCC1. Whereas their role is well established in cortical principal neurons, it remains
42 poorly documented in GABAergic interneurons. We used complementary electrophysiological
43 approaches to compare the effects of GABAAR activation in adult mouse hippocampal
44 parvalbumin interneurons (PV INs) and pyramidal cells (PCs). Loose cell attached, tight-seal
45 and gramicidin-perforated patch recordings all show GABAAR-mediated transmission is
46 slightly depolarizing and yet inhibitory in both PV INs and PCs. Focal GABA uncaging in whole-
47 cell recordings reveal that KCC2 and NKCC1 are functional in both PV INs and PCs but
48 differentially contribute to transmembrane chloride gradients in their soma and dendrites.
49 Blocking KCC2 function depolarizes the reversal potential of GABAAR-mediated currents in PV
50 INs and PCs, often beyond firing threshold, showing KCC2 is essential to maintain the
51 inhibitory effect of GABAARs. Finally, we show that repetitive 10 Hz activation of GABAARs in
52 both PV INs and PCs leads to a progressive decline of the postsynaptic response independently
53 of the ion flux direction or KCC2 function. This suggests intraneuronal chloride buildup may
54 not predominantly contribute to activity-dependent plasticity of GABAergic synapses in this
55 frequency range. Altogether our data demonstrate similar mechanisms of chloride regulation
56 in mouse hippocampal PV INs and PCs and suggest KCC2 downregulation in the pathology may
57 affect the valence of GABA signaling in both cell types.

58

59

60 **Introduction**

61 Information representation and processing in the cerebral cortex relies on the dynamic
62 interaction between ensembles of glutamatergic principal neurons and local, highly diversified
63 GABAergic interneurons (Buzsaki, 2010). These interneurons mediate feedforward and/or
64 feedback inhibition onto principal cells (PCs) and thereby control their coordinated activity
65 (Klausberger & Somogyi, 2008). In particular, parvalbumin-expressing interneurons (PV INs),
66 which receive excitatory inputs from both local and distant PCs, in turn provide them with fast
67 perisomatic inhibition (Hu *et al.*, 2014). Fast inhibitory signaling by PV INs controls the timing
68 of principal cell activity (Pouille & Scanziani, 2001) and plays a major role in the generation of
69 rhythmic activities (Klausberger & Somogyi, 2008; Amilhon *et al.*, 2015; Gan *et al.*, 2017) as
70 well as the segregation of PCs into functional assemblies (Agetsuma *et al.*, 2018). However, in
71 addition to excitatory inputs from PCs, PV INs also receive GABAergic innervation from local
72 interneurons (Chamberland & Topolnik, 2012), including some specialized in interneuron
73 inhibition (Gulyas *et al.*, 1996), as well as long-range projecting interneurons (Freund & Antal,
74 1988). Although GABAergic synapses formed onto PV INs share many properties with those
75 impinging onto principal cells, input- and cell-specific properties were also reported
76 (Chamberland & Topolnik, 2012). For instance, predominant expression of the $\alpha 1$ GABAAR
77 subunit confers PV INs with faster postsynaptic current kinetics as compared to PCs (Gao &
78 Fritschy, 1994; Bartos *et al.*, 2002).

79

80 Since GABAARs are predominantly chloride-permeable channels (Bormann *et al.*, 1987),
81 transmembrane chloride gradients also represent a major source of variability for GABA
82 signaling. Cation chloride cotransporters (CCCs) play a critical role in regulating chloride

83 gradients in neurons. Thus, the Na⁺ K⁺ Cl⁻ transporter NKCC1 and the K⁺ Cl⁻ transporter KCC2
84 are secondary active transporters that regulate intraneuronal chloride using the Na⁺ and K⁺
85 electrochemical gradients generated by the Na/K-ATPase (Blaesse *et al.*, 2009). Delayed,
86 postnatal KCC2 expression has been shown to contribute to a progressive shift in
87 intraneuronal chloride and the polarity of GABA signaling in cortical PCs *in vitro* (Rivera *et al.*,
88 1999). *In vivo*, GABA was shown to depolarize immature PCs and yet exert a predominantly
89 inhibitory action on their activity (Kirmse *et al.*, 2015), due to membrane resistance shunting.
90

91 However, much less is known regarding chloride handling in GABAergic interneurons. Thus,
92 the reversal potential of GABAAR-mediated currents (E_{GABA}) was suggested to be more
93 depolarized in unidentified hippocampal *stratum radiatum* interneurons compared with
94 neighboring PCs (Patenaude *et al.*, 2005). In addition, the driving force of GABAAR-mediated
95 currents was shown to remain unchanged during postnatal maturation, in *stratum oriens*
96 interneurons (Banke & McBain, 2006) but appear to exhibit a hyperpolarizing shift in dentate
97 gyrus basket cells (Sauer & Bartos, 2010). Although most interneurons subtypes were shown
98 to strongly express KCC2 in the adult rat hippocampus (Gulyas *et al.*, 2001), how CCC
99 expression or function control the polarity and efficacy of GABA signaling in these cells
100 remains unknown. One difficulty in addressing this question relates to the diversity and bias
101 of experimental approaches used to evaluate the effect of GABA or chloride transport with
102 minimal perturbation of the neuronal integrity. Here, we used a combination of both invasive
103 and non-invasive *in vitro* electrophysiological approaches to compare GABA signaling in
104 mouse CA1 PV INs and PCs in adult mouse hippocampus. Our results reveal that GABA
105 predominantly exerts depolarizing yet inhibitory actions over both cell types. KCC2 and NKCC1

106 appear to be functional in both PV INs and PCs even though the two cell types exhibit different
107 somato-dendritic chloride gradients. Finally, we demonstrate that CCCs do not contribute in
108 activity-dependent depression of GABAAR-mediated transmission upon moderate activation
109 frequency (10 Hz). Together our results demonstrate that, in the adult hippocampus, PV INs
110 and PCs both rely on CCC activity to maintain inhibitory GABA signaling.

111

112 **Methods**

113 *Ethical approval*

114 All procedures conformed to the International Guidelines on the ethical use of animals, the
115 French Agriculture and Forestry Ministry guidelines for handling animals (decree 87849,
116 licence A 75-05-22) and were approved by the Charles Darwin ethical committee
117 (APAFIS#4018-2015111011588776 v7).

118

119 *Animals*

120 *Pvalb*^{tm1(cre)Arbr}/J mice were crossed with *Gt(ROSA)26Sor*^{tm14(CAG-tdTomato)Hze}/J (Ai14) reporter
121 mice expressing the red fluorescent protein tdTomato. The genetic background of both
122 *Pvalb*^{tm1(cre)Arbr}/J and Ai14 mice was C57BL/6J and dual homozygous male or female mice
123 typically aged 35-70 days were used in all experiments. Mice were kept under a 12/12 hours
124 light/dark photocycle and provided with food and water *ad libitum*. Since we did not observe
125 sex-dependent differences in the biological parameters tested in this study, data from animals
126 of either sex were grouped.

127

128 *Immunohistochemistry and imaging*

129 Mice were deeply anesthetized by intraperitoneal injection of ketamine/xylazine (100/20
130 mg.kg⁻¹) and perfused transcardially with oxygenated ice-cold solution containing in mM :
131 110 choline-Cl, 2.5 KCl, 1.25 NaH₂PO₄, 25 NaHCO₃, 25 glucose, 0.5 CaCl₂, 7 MgCl₂, 11.6 ascorbic
132 acid, 3.1 Na pyruvate (~300 mOsm), equilibrated with 95% O₂-5% CO₂. Brains were removed
133 and fixed for 4-5 h at 4°C with 4% paraformaldehyde in 0.1M sodium phosphate buffer (pH

134 7.5) and cryoprotected in 30% sucrose in PBS for an additional 24h. Coronal, 40 μm -thick
135 sections were cut with a cryotome. Free-floating sections were rinsed in PBS and incubated
136 for 4 h in PBS supplemented with 0.5% Triton X-100 and 5% normal goat serum. They were
137 then incubated for 48 h at 4°C with rabbit polyclonal KCC2 antibody (1:400) diluted in PBS
138 supplemented with 0.1% Triton X-100 and 5% normal goat serum before being rinsed in PBS
139 and incubated overnight at 4°C with biotinylated WFA lectin (1:500). The sections were then
140 rinsed in PBS and then incubated for 4h with donkey anti-rabbit Cy5, rinsed in PB and
141 incubated for 40 min with streptavidin Alexa-488. After rinsing in PB, the sections were
142 mounted with Mowiol/Dabco (25 $\text{mg}\cdot\text{ml}^{-1}$) and stored at 4°C.

143

144 KCC2-immunolabeled sections were imaged with a Leica SP5 confocal microscope using a 63x
145 1.40-N.A. objective with 2X electronic magnification and Ar/Kr laser set at 488, 561 and 633
146 nm for excitation of Alexa-488, td-tomato and Cy5, respectively. Stacks of 10 optical sections
147 were acquired at a pixel resolution of 0.12 μm and a z-step of 0.29 μm .

148

149 *Electrophysiological recordings*

150 Mice were deeply anesthetized by intraperitoneal injection of ketamine/xylazine (100/20
151 $\text{mg}\cdot\text{kg}^{-1}$, Sigma-Aldrich) and transcardially perfused with ice-cold solution containing (in mM):
152 110 choline-Cl, 2.5 KCl, 1.25 NaH_2PO_4 , 25 NaHCO_3 , 25 glucose, 0.5 CaCl_2 , 7 MgCl_2 , 11.6 ascorbic
153 acid, 3.1 Na pyruvate (~ 300 mOsm), equilibrated with 95% O_2 -5% CO_2 . Mice were then
154 decapitated and 350 μm -thick parasagittal brain slices were prepared with a vibratome
155 (Microm, Thermo Scientific, France) in the same ice-cold solution and maintained in a

156 humidified interface chamber saturated with 95% O₂-5% CO₂ for 10 minutes at 34°C and then
157 at room temperature until use. Artificial cerebrospinal fluid (ACSF) for slice maintenance and
158 recording contained (in mM): 126 NaCl, 26 NaHCO₃, 10 D-glucose, 3.5 KCl, 1.6 CaCl₂, 1.2 MgCl₂,
159 1.25 NaH₂PO₄. For recordings, slices were transferred into a chamber (BadController V; Luigs
160 & Neumann) maintained at 32°C and mounted on an upright microscope (BX51WI; Olympus).
161 Slices were superfused with ACSF at a rate of 2.5 ml.min⁻¹. All recordings were performed
162 using a Multiclamp 700B amplifier (Molecular Devices).

163 Loose cell-attached recordings (seal resistance: 15-25 MΩ) were made using 4-6 MΩ
164 borosilicate glass pipettes containing normal ACSF or HEPES-buffered saline containing (in
165 mM): 150 NaCl, 3.5 KCl, 1.6 CaCl₂, 1.2 MgCl₂, 10 HEPES, pH 7.4 with NaOH (300 mOsm) in the
166 presence of excitatory transmission blockers (10 μM NBQX and 50 μM D-APV) at a holding
167 potential of 0 mV. Recordings were established by gently pushing the pipette against the
168 membrane of the cell. Signals were filtered at 4 kHz and acquired using pClamp software
169 (Molecular Devices) in voltage clamp mode at a sampling rate of 10-20 kHz.

170

171 Tight cell-attached recordings (Perkins, 2006) were performed in the presence of 10 μM NBQX
172 and 50 μM D-APV under current-clamp configuration (I=0 mode) to evaluate the polarity of
173 GABAAR-mediated potentials. Recording pipettes (4-9 MΩ) were filled with the HEPES-
174 buffered saline. Seal resistance in the cell-attached mode was >4 GΩ. Voltage signals were
175 filtered at 4 kHz and sampled at 10-20 kHz.

176

177 For whole-cell recordings, pipettes (3–5 MΩ resistance) were filled with a solution containing
178 (in mM): 115 K-gluconate, 25.4 KCl, 10 HEPES, 10 EGTA, 1.8 MgCl₂, 2 Mg-ATP, 0.4 Na₃-GTP, pH

179 7.4 (290 mOsm) supplemented with Alexa 594 (20 μ M) to check cell morphology. Images of
180 the soma and dendrites were acquired at least 15 min after break in, using 535 nm excitation
181 light (CoolLED) to prevent RuBi-GABA uncaging. Cells were voltage-clamped at -60 or -70 mV.
182 Voltage was corrected *post hoc* for liquid junction potential (-11 mV) and voltage drop across
183 the series resistance (<25 M Ω) of the pipette. Currents were filtered at 4 kHz and sampled at
184 10 kHz.

185 For gramicidin-perforated patch recordings, the tip of the recording pipette was filled with
186 gramicidin-free solution containing (in mM): 120 KCl, 10 HEPES, 11 EGTA, 1 CaCl₂, 2 MgCl₂, 35
187 KOH, 30 glucose adjusted to pH 7.3 with KOH (300 mOsm). The pipette was then backfilled
188 with the same solution containing 100 μ g/ml gramicidin and 20 μ M Alexa 488 to verify
189 membrane integrity during the recording. Gramicidin was prepared as a stock solution at 50
190 mg/ml in DMSO. Pipette resistance was 4-5 M Ω . Cells were voltage-clamped at -70 mV.
191 Recordings were started once series resistance was less than 100 M Ω (52.5 \pm 7.6 M Ω for PV INs
192 (n=10) and 69.1 \pm 5.8 M Ω for PCs (n=16)). The Donnan potential between the pipette solution
193 and cell cytoplasm was measured (Kim & Trussell, 2007) after spontaneous membrane rupture
194 (11.7 \pm 1.1 mV; n = 4). The Donnan potential was partly offset by a liquid junction potential of
195 -4 mV. Therefore, the holding potential in gramicidin-perforated recordings reads 7.7 mV
196 more hyperpolarized than the actual membrane potential. Potentials were corrected *post hoc*
197 for this residual potential and voltage drop across the series resistance of the pipette.
198 Spontaneous action potentials (APs) and resting membrane potential (V_m) were monitored
199 under current clamp configuration (I=0 mode) while E_{GABA} was measured by RuBi-GABA
200 photolysis under voltage clamp. V_m was estimated by averaging membrane potential every
201 500 ms for 30-60 sec in normal ACSF. Membrane potential in the presence of drugs for
202 photolysis were similarly computed over 30-60 sec (Fig. 6A). The threshold for action potential

203 initiation was determined from the first peak in the third derivative of action potential
204 waveforms averaged from > 4 APs (Henze & Buzsaki, 2001). Currents were filtered at 10 kHz
205 and sampled at 10-20 kHz.

206

207 *Photolysis*

208 Photolysis of RuBi-GABA (15 μ M) onto parvalbumin positive interneurons (PV INs) or
209 pyramidal cells (PCs) was performed in the presence of 10 μ M NBQX, 50 μ M D-APV, 2 μ M
210 CGP55845 and 1 μ M tetrodotoxin (TTX). A 405 nm laser diode beam (Deepstar, Omicron,
211 Photon Lines, France) conducted through a multimode optic fibre and alignment device
212 (Prairie Technologies, Middleton, WI, USA) was set to generate a 3-5 μ m spot in the objective
213 focus and directed to the soma or distal dendrites of the recorded neurons. The power of the
214 laser head output was controlled using Omicron Laser Controller v2.97, while trigger and pulse
215 duration were set using pClamp software and a Digidata controller. Photolysis was induced by
216 a 0.5-1 msec pulse at 10 mW on the soma or 3-5 msec at 10 mW on distal dendrites. Series of
217 15 s voltage steps with a 5 mV increment were applied to the pipette with an inter-episode
218 interval of 40 sec. Laser pulses were delivered at 12 sec after the onset of the voltage step to
219 allow for stabilization of the holding current. The amplitude of GABA-evoked currents was
220 computed as the difference between the current measured over a 4 ms window centered on
221 the peak and the baseline current averaged over 3 ms prior to the laser flash. The distance
222 from soma for dendritic uncaging was measured offline with NeuronJ (Meijering *et al.*, 2004),
223 based on Alexa 594 fluorescence imaging of the recorded neuron.

224

225 *Drug application*

226 Isoguvacine (100 μ M; Tocris Bioscience) was dissolved in normal ACSF supplemented with 2
227 μ M Alexa 488 to detect regions puffed through a patch pipette using a Picosplitzer III (5 sec at
228 10 psi). All other drugs were bath applied: NBQX, D-AP5, were from Hello Bio (Bristol, UK).
229 Isoguvacine, RuBi-GABA trimethylphosphine, CGP55845, VU0463271 were from Tocris
230 Bioscience (Bristol, UK). TTX was from Latoxan. All other drugs were from Sigma-Aldrich
231 France. CGP55845, VU0463271 and bumetanide were dissolved in DMSO for stock solutions.

232

233 *Data analysis*

234 Electrophysiological data analysis was performed offline using Clampfit 10 (Molecular Devices,
235 USA) and custom routines written in Igor Pro 6 (WaveMetrics, USA).

236

237 **Statistical analysis**

238 The results are presented as mean \pm standard deviation throughout the manuscript and in all
239 figures. For statistical analyses, non-parametric Mann-Whitney or Wilcoxon signed-rank tests
240 were used unless Shapiro-Wilk normality test was passed and Student's t-test could be used.
241 Multiple linear regression analysis was performed using SigmaPlot 12,5 (SPSS). χ^2 tests were
242 computed using Excel spreadsheets. Statistical significance was set at $p < 0.05$.

243

244

245

246

247

248

249 **Results**

250 **KCC2 expression in hippocampal parvalbumin interneurons**

251 Although the expression and function of CCCs are well characterized in hippocampal principal
252 neurons, whether they are expressed and functional in GABAergic interneurons remains
253 largely unexplored. We used immunohistochemistry in *Pvalb^{tm1(cre)Arbr/J::Ai14}* mice to
254 investigate KCC2 expression in mouse hippocampal parvalbumin interneurons (PV Ins) (Le
255 Roux *et al.*, 2013).

256

257 In all hippocampal subfields, KCC2 expression was observed in td-tomato-positive
258 interneurons (Figure 1A). As in PCs, KCC2 immunostaining in PV INs was mostly pericellular,
259 likely reflecting predominant membrane expression (Figure 1B). However, KCC2 expression in
260 PV INs was sometimes difficult to distinguish from that in neighboring PCs. To circumvent this
261 problem, we used extracellular matrix staining to precisely visualize PV IN contours.
262 Hippocampal PV INs somata and proximal dendrites are wrapped by a chondroitin sulfate
263 proteoglycan-rich extracellular matrix, called perineuronal net (PNN) (Hartig *et al.*, 1992). Thus
264 using specific staining of PNNs with Wisteria Floribunda Agglutinin (WFA), KCC2
265 immunostaining in PV INs could be distinguished from that in adjacent principal neurons as it
266 was surrounded by WFA staining, further confirming KCC2 expression in PV INs (Figure 1B).

267 These results support the conclusion that KCC2 protein is expressed at the membrane of PV
268 INs in the adult mouse hippocampus.

269 (Figure 1 near here)

270 **Net effect of GABAAR activation on CA1 pyramidal neurons and parvalbumin interneurons.**

271 We next asked whether cation-chloride cotransporters are functional in CA1 PV INs and how
272 they influence GABAAR-mediated signaling in these cells. Loose cell-attached recordings allow
273 detection of action potentials from identified neurons with minimal perturbation of their
274 physiology (Llano & Marty, 1995). We first used this approach to evaluate the excitatory vs.
275 inhibitory nature of GABA transmission in CA1 PV INs and neighboring pyramidal neurons
276 (PCs). The effect of GABAAR activation was tested by locally puffing the GABAAR agonist
277 isoguvacin (100 μ M, 5 s) onto the soma of the recorded cell. In order to prevent the influence
278 of polysynaptic EPSPs, recordings were performed in the presence of AMPA and NMDA
279 receptor antagonists. Under these conditions however only a few (5 of 27) PV INs exhibited
280 spontaneous firing (Figure 2A). Out of 27 recorded PV INs, isoguvacine induced firing in 1,
281 blocked firing in 5 and had no detectable effect in 21 interneurons. The KCC2 specific
282 antagonist VU0463271 (10 μ M) significantly increased the proportion of PV INs that were
283 excited or inhibited by isoguvacine (χ^2 test, $0.01 < p < 0.02$) whereas the NKCC1 antagonist
284 bumetanide (10 μ M) had no significant effect on the proportions of each type of response,
285 either when applied alone (χ^2 test, $0.05 < p < 0.1$) or in the presence of VU0463271 (χ^2 test,
286 $0.95 < p < 0.98$). These results suggest the effect of GABAA receptor activation is predominantly
287 inhibitory in PV INs and is influenced by the function of KCC2 but not NKCC1.

288 (figure 2 near here)

289 In neighboring PCs, isoguvacine had little effect on firing (5 of 23 cells), mostly owing to the
290 fact that most of them were silent (18 of 23 cells) prior to isoguvacine application, making it
291 difficult to assess the inhibitory or excitatory nature of GABA signaling. Again, bumetanide had
292 no significant effect on the proportions of pyramidal cells excited (1 of 10 cells), inhibited (1
293 of 10 cells) or unaffected by isoguvacine (χ^2 test, $0.2 < p < 0.8$), whereas VU0463271 induced a

294 large increase in the proportion of excited neurons (7 of 11 cells, χ^2 test, $0.01 < p < 0.02$; Figure
295 2D). In contrast, in slices from younger (3-7 days old) animals, the effect of isoguvacine was
296 significantly more excitatory than in slices from adult mice (χ^2 test, $0.02 < p < 0.05$) and triggered
297 firing in 26 out of 66 neurons under control conditions, suggesting GABA signaling in PCs was
298 clearly excitatory at this age.

299

300 Altogether, these results suggest KCC2 is functional in both CA1 pyramidal cells and PV INs and
301 influences the valence of GABA signaling. However, the high proportion of silent neurons
302 under our recording conditions makes it difficult to draw firm conclusions regarding the
303 polarity of GABA transmission in these cells under physiological conditions.

304

305 Tight-seal, cell-attached recordings provide another, minimally invasive approach to detect
306 the polarity of synaptic potentials without rupturing the cell membrane and perturbing
307 transmembrane ionic gradients (Perkins, 2006). In particular, gigaseal recordings allow a fairly
308 reliable measurement of the polarity (but not the actual amplitude) of synaptic potentials, as
309 well as of resting membrane potential, provided that series resistance is high relative to patch
310 and cell membrane resistances (Mason *et al.*, 2005; Perkins, 2006). We recorded currents
311 evoked by GABAAR activation with isoguvacine in gigaseal mode from both CA1 PV INs and
312 PCs (Figure 3A). In both cell types, isoguvacine-induced potentials were predominantly
313 depolarizing (5 of 7 and 5 of 6 cells, respectively). This proportion was similar to recordings
314 from immature (P3-P7) CA1 pyramidal neurons (6 of 9 cells, Figure 3B). Together, these results
315 suggest that, at least in the absence of glutamatergic drive, both CA1 PCs and PV INs are
316 predominantly depolarized upon GABAAR activation, even though a significant fraction are

317 functionally inhibited, likely due to shunting of their membrane resistance (Staley & Mody,
318 1992).

319 (Figure 3 near here)

320 **KCC2-mediated chloride extrusion in CA1 parvalbumin interneurons**

321 Transmembrane chloride transport can be directly estimated from whole-cell recordings of
322 GABA-evoked currents while clamping somatic chloride concentration to 29 mM (Khirug et al.,
323 2008; Gauvain et al., 2011). The gradient of the reversal potential of GABAAR-mediated
324 currents (E_{GABA}) along the somato-dendritic membrane then reflects actual transmembrane
325 chloride extrusion. We compared E_{GABA} gradients in CA1 PV INs and PCs using local photolysis
326 of RubiGABA (15 μ M, 0.5-5 ms laser pulse, see Methods). As in other cortical neurons (Khirug
327 et al., 2008; Gauvain et al., 2011), E_{GABA} in PV INs, was always more depolarized for somatically-
328 evoked currents, as compared to currents evoked onto dendrites 50-250 μ m away from the
329 soma (Figure 4). This somato -dendritic gradient (ΔE_{GABA}) however was significantly steeper in
330 neighboring PCs as compared with PV INs (-21.1 ± 5.7 vs -12.6 ± 2.8 mV/100 μ m; 11 dendritic
331 sites in 8 cells and 17 dendritic sites in 9 cells, respectively, $p < 0.001$; Figure 5A-B), suggesting
332 chloride extrusion along dendrites may be less effective in PV INs. However, the effect of KCC2
333 and NKCC1 blockers on ΔE_{GABA} was not significantly different between the two cell types. Thus,
334 the KCC2 specific antagonist VU046321 produced similar reduction in the somato-dendritic
335 gradient of E_{GABA} in PV INs (-58.5 ± 11.6 %, 15 dendritic sites in 9 cells) and PCs (-57.1 ± 8.1 %,
336 9 dendritic sites in 7 cells, $p = 0.770$; Figure 4B and 5C). Further application of the NKCC1
337 antagonist bumetanide also produced similar increase in ΔE_{GABA} in PV INs and PCs ($+41.5 \pm$
338 23.9 % and $+45.7 \pm 28.2$, respectively, as compared to VU046321 only; $p = 0.67$, Figure 5C). This
339 suggests NKCC1 activity may significantly contribute to transmembrane chloride gradients in

340 both cell types, at least upon KCC2 blockade. Altogether, these observations demonstrate
341 chloride extrusion is more efficient along the dendrites of PCs as compared with PV INs and
342 suggest mechanisms other than CCC function may contribute to this difference.

343 (Figure 4 near here)

344 Remarkably, although somatic chloride concentration was expected to be clamped by the
345 internal solution of the pipette, somatic E_{GABA} was more hyperpolarized than that estimated
346 by the Nernst equation (-41.3 mV, dashed line in Figure 5D) and more so in PV INs than PCs
347 (53.1 ± 3.4 vs 46.5 ± 2.5 mV, $n=10$ and 8 cells, respectively, $p=0.003$; Figure 5D). This suggests
348 that active chloride transport at the plasma membrane i) may generate intracellular chloride
349 gradients, such that actual transmembrane gradients do not directly reflect the mean
350 intracellular and extracellular concentrations and ii) is more efficient in the soma of PV INs
351 than in PCs. Consistent with this hypothesis, somatic E_{GABA} was more depolarized upon
352 application of VU0463271 in PV INs than in PCs ($+4.9 \pm 1.7$ vs $+2.8 \pm 1.6$ mV, $n=9$ and 7 cells,
353 respectively, $p=0.039$; Figure 5E). Further application of bumetanide however had no
354 significant effect on E_{GABA} in either cell type, suggesting NKCC1 does not contribute
355 significantly to somatic transmembrane chloride gradients when intracellular chloride
356 concentration is high (-0.43 ± 1.1 vs -0.71 ± 1.9 mV, $n=8$ and 7 cells, respectively, $p=0.95$;
357 Figure 5E). Altogether, our results demonstrate that KCC2 and NKCC1 are functional in PCs and
358 PV-INs and contribute to establish steady-state transmembrane chloride gradients. The
359 relative contribution of each transporter to somatic gradients however differ between PV INs
360 and PCs.

361 (Figure 5 near here)

362 In order to assess both E_{GABA} and V_m while minimizing perturbation of intracellular anion
363 homeostasis, we next used gramicidin-perforated patch recordings. First, we measured V_m
364 and tested the effect of pharmacologically blocking the excitatory drive onto CA1 PV INs and
365 PCs, as in experiments shown in Figure 2 and 3. Whereas all PV INs were spontaneously firing
366 at rest (frequency: 4.0 ± 5.2 Hz, $n=14$ cells), application of AMPA and NMDAR blockers
367 hyperpolarized their membrane potential by 3.5 ± 2.2 mV (Figure 6A and 6Bb). Most PCs (12
368 out of 15) were also spontaneously firing but had lower firing frequency (0.23 ± 0.3 Hz,
369 $p<0.001$) and threshold ($p=0.006$) (Figure 6A and 6Bc). Glutamate receptor antagonists also
370 hyperpolarized CA1 pyramidal cells, yet to a lesser extent than PV INs (0.96 ± 1.2 mV, $p=0.001$,
371 $n= 13$ cells of each type, Figure 6Bb), consistent with the latter receiving massive excitatory
372 drive as compared with neighboring pyramidal cells (Gulyas *et al.*, 1999; Takacs *et al.*, 2012).
373 Remarkably, these values of V_m measured in the presence of glutamate receptor antagonists
374 were very similar to those derived from gigaseal recordings (71.6 ± 2.1 vs -74.9 ± 5.2 mV ($n=7$)
375 for PV INs and vs -74.9 ± 4.5 ($n=8$) for PCs; Figure 3). GABAAR-mediated currents were then
376 evoked using focal uncaging of RubiGABA, as above, and E_{GABA} was derived from current-
377 voltage relations of somatically evoked currents (Figure 6C-D). E_{GABA} was significantly more
378 depolarized in PV INs as compared with PCs (-64.1 ± 7.2 vs -71.7 ± 3.0 mV, $p=0.003$, $n= 10$ and
379 16 cells, respectively; Figure 6E). However, due to more depolarized V_m in PV INs (Figure 6Ba),
380 the driving force of GABAAR-mediated currents at rest was similar in the two cell types ($3.8 \pm$
381 7.0 vs 1.7 ± 3.7 mV, $n=10$ and 13 cells, respectively; $p=0.34$; Figure 6F). Also consistent with
382 gigaseal recordings, E_{GABA} was slightly more depolarized than V_m both in PV INs and PCs.
383 Application of VU0463271 depolarized somatic E_{GABA} in both cell types (by 12.5 ± 2.8 and 16.1
384 ± 4.2 mV, in PV INs ($n=3$) and PCs ($n=8$), respectively; Figure 6G) whereas further application
385 of bumetanide only slightly hyperpolarized E_{GABA} . This suggests that, under steady-state

386 conditions, E_{GABA} in both PV INs and PCs is moderately depolarized as compared with V_m and
387 predominantly influenced by the activity of KCC2, whereas NKCC1 contribution is minor.
388 Importantly, however, although GABA may have depolarizing actions in both cells types, its
389 effect is mostly shunting as E_{GABA} is more hyperpolarized than the action potential threshold
390 (Figure 6H). Suppressing KCC2 activity may however be sufficient to depolarize E_{GABA} beyond
391 this threshold, thereby promoting firing, as observed in Figure 2.

392 (Figure 6 near here)

393 **Dynamic regulation of GABA signaling in CA1 parvalbumin interneurons and pyramidal cells**

394 Repetitive activation of GABAARs has been shown in a variety of neurons to result in activity-
395 dependent depression. This depression was attributed to intracellular chloride buildup
396 (Thompson & Gahwiler, 1989a; Staley & Proctor, 1999; Jedlicka *et al.*, 2011) or to receptor
397 desensitization (Thompson & Gahwiler, 1989c; Jones & Westbrook, 1995) or a combination of
398 both. We compared the contribution of these mechanisms upon repetitive activation of
399 GABAARs in CA1 PV INs and neighboring PCs. In order to exclude presynaptic mechanisms that
400 may contribute to short-term, activity-dependent changes in GABA release (Thompson &
401 Gahwiler, 1989c; Zucker & Regehr, 2002), GABAAR activation was achieved by repetitive (10
402 Hz), focal uncaging of RubiGABA onto the soma or dendrites of neurons recorded in
403 gramicidin-perforated patch mode (Figure 7A). We then compared the dynamics of GABAAR-
404 mediated currents evoked while holding cells below (-8.2 ± 3.3 mV) or above ($+9.4 \pm 3.6$ mV)
405 their reversal potential, such that the absolute amplitude of the first response was similar for
406 inward and outward currents. Both in PV INs and PCs, the peak amplitude of GABAAR-
407 mediated currents decayed with very similar kinetics during the train, independent of their
408 polarity (soma: $\tau_{inward}=0.11 \pm 0.03$ vs 0.17 ± 0.12 s⁻¹, Mann-Whitney test $p=0.291$; $\tau_{outward}=0.10$

409 ± 0.04 vs 0.13 ± 0.03 s⁻¹, Mann-Whitney test p=0.232; n=6 and 11 cells, respectively) and their
410 site of initiation (soma vs dendrite; $0.242 < p < 0.695$; Figure 7B). This observation suggests the
411 mechanisms involved in the activity-dependent depression of GABAAR-mediated currents
412 during a train of 10 Hz stimulation is unlikely to primarily involve changes in transmembrane
413 ionic gradients. Consistent with this conclusion, application of the KCC2 antagonist
414 VU0463271 had no detectable effect on the decay of outward GABAAR-mediated currents,
415 either in PV INs ($\tau_{\text{outward}}=0.13 \pm 0.04$ vs 0.11 ± 0.06 s⁻¹, paired t-test p=0.363; n=2 cells) or in
416 PCs ($\tau_{\text{outward}}=0.11 \pm 0.02$ vs 0.11 ± 0.01 s⁻¹, paired t-test p=0.848; n=4 cells ; Figure 7C). We
417 conclude that, at least in our range of current amplitude and stimulation frequency, activity-
418 dependent depression of GABAAR-mediated currents is largely independent of CCC function
419 and does not reflect changes in transmembrane chloride gradients.

420 (Figure 7 near here)

421 Discussion

422 We have used a combination of approaches to assess and compare the polarity of GABA
423 signaling in adult mouse CA1 hippocampal PCs and PV INs. Our results reveal that the basic
424 mechanisms of steady-state chloride handling controlling GABA transmission are similar in
425 both neuronal types, with a predominantly depolarizing yet inhibitory effect under resting *in*
426 *vitro* conditions. PV INs and PCs, however, show different behaviors upon intracellular chloride
427 loading, that may reflect differential distribution, regulation or efficacy of cation chloride
428 cotransport along their somato-dendritic axis as well as electrotonic properties. Finally, we
429 have shown that activity-dependent depression of GABAR-mediated transmission is largely
430 independent of the polarity of the evoked currents and the activity of the transporters. This
431 suggests this form of plasticity may not predominantly involve postsynaptic chloride loading,
432 at least under moderate regimes of synaptic activation.

433

434 Evaluating the net effect of GABAAR activation in neurons is technically challenging as all
435 experimental approaches may introduce some bias. Classical electrophysiological techniques
436 may induce cell dialysis, compromise membrane integrity or underestimate Donnan
437 potentials between pipette solution and the neuronal cytoplasm (Marty & Neher, 1995). Non-
438 invasive approaches, such as loose-patch recordings, are then often used to assess the polarity
439 and/or the net effect of GABAAR activation on neuronal activity (Deidda *et al.*, 2015; Lozovaya
440 *et al.*, 2019). This approach, however, is only valid when recorded cells display spontaneous
441 firing. As focal application of GABAAR agonists may affect the activity of neighboring neurons
442 and subsequently modify that of the recorded neuron, we performed these recordings in the
443 presence of glutamate receptor antagonists (Fig. 2). In the absence of excitatory drive,

444 however, most recorded neurons (either PV INs or PCs) did not exhibit spontaneous firing and
445 the effect of GABAAR activation could not be tested. These experiments nevertheless showed
446 that GABA agonists mostly inhibit spontaneously firing PV INs. Cell-attached current clamp
447 recordings provide another, minimally invasive approach to evaluate the polarity of synaptic
448 potentials as well as resting membrane potential (Perkins, 2006; Kirmse *et al.*, 2015). Such
449 recordings showed that GABAAR activation mostly induces membrane depolarization in both
450 PV INs and PCs in adult mouse hippocampus, as well as in PCs from immature (P3-7)
451 hippocampus. This observation is supported by gramicidin-perforated patch recordings, which
452 revealed a depolarizing driving force for GABAAR-mediated currents (Fig. 6). Although E_{GABA}
453 was more depolarized in CA1 PV INs than in neighboring PCs, the driving force of GABAAR-
454 mediated currents was remarkably similar, due to a more depolarized resting membrane
455 potential in PV INs. This observation is consistent with previous recordings from presumptive
456 basket (fast spiking) and pyramidal (regular spiking) neurons in both amygdala and cortex
457 (Martina *et al.*, 2001). Importantly, under control conditions, E_{GABA} was less depolarized than
458 action potential threshold (Fig. 6H), consistent with a predominantly shunting and inhibitory
459 effect. This observation is in line with earlier studies on cerebellar interneurons (Chavas &
460 Marty, 2003), unidentified hippocampal interneurons (Verheugen *et al.*, 1999; Banke &
461 McBain, 2006) as well as presumptive dentate gyrus PV INs (Sauer & Bartos, 2010).

462

463 Very few studies have explored CCC expression in cortical interneurons and data are
464 somewhat controversial, possibly due to the differential expression of distinct isoforms
465 (Uvarov *et al.*, 2007; Markkanen *et al.*, 2014). Thus, KCC2 was shown to be expressed in MGE-
466 derived interneurons earlier than in neighboring pyramidal cells during embryogenesis and to

467 control the termination of their migration (Bortone & Polleux, 2009). However, KCC2
468 expression and function in specific MGE-derived subtypes in postnatal cortex have not been
469 further explored. In the cerebellum on the contrary, KCC2 expression is very weak in early
470 postnatal presumptive baskets cells and increases postnatally (Simat *et al.*, 2007). In the adult
471 rat hippocampus, KCC2 was shown to be strongly expressed in PV-immunopositive
472 interneurons (Gulyas *et al.*, 2001), consistent with our immunohistochemical data (Fig. 1). Due
473 to the delayed expression of parvalbumin in PV INs (Solbach & Celio, 1991), we could not,
474 however, visualize CA1 PV INs in PVCre::Ai14 mice in early postnatal mice and therefore could
475 not evaluate the temporal profile of KCC2 expression and function in these cells at earlier
476 stages. In addition, the lack of a specific NKCC1 antibody for immunohistochemistry precluded
477 examination of NKCC1 expression in PV INs and PCs. Our pharmacological data, however,
478 support that both transporters are expressed and functional in both cell types in PV INs and
479 PCs in the adult mouse hippocampus. Thus, the KCC2 antagonist VU0463271 and the NKCC1
480 antagonist bumetanide had opposing actions on the efficacy of transmembrane chloride
481 export (Fig. 5) and E_{GABA} (Fig. 6) in both PV INs and PCs. However, blocking KCC2 was sufficient
482 to promote the excitatory effect of GABAAR activation whereas blocking NKCC1 had not
483 detectable effect (Fig 2), suggesting although both transporters are active in PV INs and PCs,
484 the valence of GABA signaling in both cell types predominantly relies on KCC2 but not NKCC1
485 function. Moreover, although KCC2 and NKCC1 blockade had similar effects on somatic E_{GABA}
486 in PV INs and PCs in perforated-patch recordings (Fig. 6G), we observed significant differences
487 when cells were loaded with high intracellular chloride in whole-cell mode. Thus, the somato-
488 dendritic gradient of E_{GABA} was more pronounced in PCs than in PV INs (Fig. 5A-B) and somatic
489 chloride extrusion was more efficient in PV INs than in PCs. These differences are consistent
490 with a differential expression and/or function of KCC2 and NKCC1 along the somato-dendritic

491 axis of the two cell types, with a higher KCC2/NKCC1 function ratio in the soma of PV INs. In
492 addition, differences in the cable properties of PV IN and PC dendrites may also contribute to
493 this difference. Thus, lower membrane resistance of PV IN as compared to PC dendrites
494 (Norenberg *et al.*, 2010) may induce poorer space clamp of GABAAR-mediated currents
495 evoked onto their distal dendrites. It should also be noted that, whereas the whole-cell
496 evaluation of E_{GABA} gradients is an effective method to assess the efficacy of transmembrane
497 chloride transport (Khirug *et al.*, 2008; Gauvain *et al.*, 2011), it may tend to overestimate
498 steady-state KCC2/NKCC1 function ratio, as it uses high intracellular chloride concentration.
499 This in turn is expected to inhibit the chloride-sensitive with-no-lysine (WNK) STE20 (sterile
500 20)-like kinases (SPAK) kinases, resulting in reduced NKCC1 and increased KCC2 function (de
501 Los Heros *et al.*, 2014; Friedel *et al.*, 2015; Heubl *et al.*, 2017).

502

503 Activity-dependent depression of GABAAR-mediated transmission is well-documented and
504 likely results from a combination of factors involving both pre- and postsynaptic elements
505 (Thompson & Gahwiler, 1989a, b, c). In particular, several studies suggested repetitive
506 activation of GABAARs may lead to postsynaptic chloride loading and a subsequent
507 depolarization of E_{GABA} (Thompson & Gahwiler, 1989a; Kaila *et al.*, 1997; Staley & Proctor,
508 1999; Magloire *et al.*, 2019). However, these studies used massive chloride loading induced
509 either by multi-quantal IPSCs or prolonged, high-frequency stimulation. Although such intense
510 receptor activation may be relevant to specific, mostly pathological conditions (Magloire *et al.*,
511 2019), it may not represent the receptor activation at individual, somatic or dendritic sites.
512 Our results from gramicidin-perforated patch recordings instead show that, upon 10 Hz focal
513 Rubi-GABA uncaging for up to 1s, GABAAR-mediated currents decay in amplitude in both PV

514 INs and PCs largely independent of both the direction of the ion flux and KCC2 function (Fig.
515 7). These results suggest that chloride accumulation during repetitive (10 Hz) activation at
516 single somatic or dendritic sites is not sufficient to significantly affect the driving force of
517 GABAAR-mediated currents, likely owing to the rapid diffusion of chloride ions inside the
518 postsynaptic cytoplasm (Doyon *et al.*, 2011). Instead, since these experiments were
519 performed independent of synaptic stimulation, activity-dependent depression of GABAAR-
520 mediated currents likely reflected receptor desensitization (Jones & Westbrook, 1996; Papke
521 *et al.*, 2011; Gielen *et al.*, 2015). Our results demonstrate this process occurs with a time
522 constant of about 100-130 ms, consistent with the intermediate component of the
523 desensitization kinetics of recombinant $\alpha_1\beta_{1/2}\gamma_2L$ receptors (Papke *et al.*, 2011; Brodzki *et al.*,
524 2016). Therefore, under physiological regimes of synaptic activity, GABAAR desensitization
525 appears as a major postsynaptic factor acting as a low-pass filter with respect to GABA
526 signaling (Jones & Westbrook, 1996).

527

528 CCC expression is altered in a variety of neurological and psychiatric conditions including
529 epilepsy (Palma *et al.*, 2006; Huberfeld *et al.*, 2007; Karlocai *et al.*, 2016; Kourdougli *et al.*,
530 2017), chronic stress (MacKenzie & Maguire, 2015), Rett syndrome (Duarte *et al.*, 2013;
531 Banerjee *et al.*, 2016; Tang *et al.*, 2016) and autism spectrum disorders (Tyzio *et al.*, 2014).
532 Impaired chloride homeostasis has been suggested to induce paradoxical excitatory GABA
533 signaling and thereby promote anomalous ensemble activities that underlie the pathology.
534 Our data also suggest that KCC2 downregulation may be sufficient to depolarize EGABA above
535 action potential threshold in PV INs (Fig. 6H). In addition, since KCC2 is involved in a variety of
536 molecular interactions with synaptic proteins (Ivakine *et al.*, 2013; Mahadevan *et al.*, 2014),

537 ion channels (Goutierre *et al.*, 2019) and cytoskeleton-related proteins (Li *et al.*, 2007; Gauvain
538 *et al.*, 2011; Chevy *et al.*, 2015; Llano *et al.*, 2015), the loss of its expression also affects several
539 physiological properties beyond the mere control of chloride transport and GABA signaling
540 (Chamma *et al.*, 2012). Thus, KCC2 knockdown in cortical PCs was shown to also profoundly
541 perturb neuronal excitability as well as network activity (Kelley *et al.*, 2018; Goutierre *et al.*,
542 2019). Since PV INs exert a critical control over the activity of cortical PCs (Pouille & Scanziani,
543 2001) and shape their rhythmic activities (Klausberger & Somogyi, 2008; Amilhon *et al.*, 2015;
544 Gan *et al.*, 2017), altered CCC expression in these cells would be expected to profoundly
545 perturb cortical rhythmogenesis. As most studies on CCC expression in the pathology lacked
546 cell-subtype resolution, whether and how it is affected in PV INs remains to be fully explored
547 and the consequences on cortical activity should then be further investigated.

548

549 **References**

- 550 Agetsuma M, Hamm JP, Tao K, Fujisawa S & Yuste R. (2018). Parvalbumin-Positive
551 Interneurons Regulate Neuronal Ensembles in Visual Cortex. *Cereb Cortex* **28**, 1831-1845.
552
- 553 Amilhon B, Huh CY, Manseau F, Ducharme G, Nichol H, Adamantidis A & Williams S. (2015).
554 Parvalbumin Interneurons of Hippocampus Tune Population Activity at Theta Frequency.
555 *Neuron* **86**, 1277-1289.
556
- 557 Banerjee A, Rikhye RV, Breton-Provencher V, Tang X, Li C, Li K, Runyan CA, Fu Z, Jaenisch R &
558 Sur M. (2016). Jointly reduced inhibition and excitation underlies circuit-wide changes in
559 cortical processing in Rett syndrome. *Proceedings of the National Academy of Sciences of the*
560 *United States of America*.
561
- 562 Banke TG & McBain CJ. (2006). GABAergic input onto CA3 hippocampal interneurons
563 remains shunting throughout development. *The Journal of neuroscience : the official journal*
564 *of the Society for Neuroscience* **26**, 11720-11725.
565
- 566 Bartos M, Vida I, Frotscher M, Meyer A, Monyer H, Geiger JR & Jonas P. (2002). Fast synaptic
567 inhibition promotes synchronized gamma oscillations in hippocampal interneuron networks.
568 *Proceedings of the National Academy of Sciences of the United States of America* **99**, 13222-
569 13227.
570

571 Blaesse P, Airaksinen MS, Rivera C & Kaila K. (2009). Cation-chloride cotransporters and
572 neuronal function. *Neuron* **61**, 820-838.

573

574 Bormann J, Hamill OP & Sakmann B. (1987). Mechanism of anion permeation through
575 channels gated by glycine and gamma-aminobutyric acid in mouse cultured spinal neurones.
576 *The Journal of physiology* **385**, 243-286.

577

578 Bortone D & Polleux F. (2009). KCC2 expression promotes the termination of cortical
579 interneuron migration in a voltage-sensitive calcium-dependent manner. *Neuron* **62**, 53-71.

580

581 Brodzki M, Rutkowski R, Jatczak M, Kisiel M, Czyzewska MM & Mozrzymas JW. (2016).
582 Comparison of kinetic and pharmacological profiles of recombinant alpha1gamma2L and
583 alpha1beta2gamma2L GABAA receptors - A clue to the role of intersubunit interactions.
584 *European journal of pharmacology* **784**, 81-89.

585

586 Buzsaki G. (2010). Neural syntax: cell assemblies, synapsembles, and readers. *Neuron* **68**,
587 362-385.

588

589 Chamberland S & Topolnik L. (2012). Inhibitory control of hippocampal inhibitory neurons.
590 *Frontiers in neuroscience* **6**, 165.

591

592 Chamma I, Chevy Q, Poncer JC & Levi S. (2012). Role of the neuronal K-Cl co-transporter
593 KCC2 in inhibitory and excitatory neurotransmission. *Frontiers in cellular neuroscience* **6**, 5.

594

595 Chavas J & Marty A. (2003). Coexistence of excitatory and inhibitory GABA synapses in the
596 cerebellar interneuron network. *The Journal of neuroscience : the official journal of the*
597 *Society for Neuroscience* **23**, 2019-2031.

598

599 Chevy Q, Heubl M, Goutierre M, Backer S, Moutkine I, Eugene E, Bloch-Gallego E, Levi S &
600 Poncer JC. (2015). KCC2 Gates Activity-Driven AMPA Receptor Traffic through Cofilin
601 Phosphorylation. *The Journal of neuroscience : the official journal of the Society for*
602 *Neuroscience* **35**, 15772-15786.

603

604 de Los Heros P, Alessi DR, Gourlay R, Campbell DG, Deak M, Macartney TJ, Kahle KT & Zhang
605 J. (2014). The WNK-regulated SPAK/OSR1 kinases directly phosphorylate and inhibit the K+
606 Cl- co-transporters. *The Biochemical journal* **458**, 559-573.

607

608 Deidda G, Parrini M, Naskar S, Bozarth IF, Contestabile A & Cancedda L. (2015). Reversing
609 excitatory GABAAR signaling restores synaptic plasticity and memory in a mouse model of
610 Down syndrome. *Nature medicine* **21**, 318-326.

611

612 Doyon N, Prescott SA, Castonguay A, Godin AG, Kroger H & De Koninck Y. (2011). Efficacy of
613 synaptic inhibition depends on multiple, dynamically interacting mechanisms implicated in
614 chloride homeostasis. *PLoS computational biology* **7**, e1002149.

615

616 Duarte ST, Armstrong J, Roche A, Ortez C, Perez A, O'Callaghan Mdel M, Pereira A, Sanmarti
617 F, Ormazabal A, Artuch R, Pineda M & Garcia-Cazorla A. (2013). Abnormal expression of
618 cerebrospinal fluid cation chloride cotransporters in patients with Rett syndrome. *PLoS one* **8**,
619 e68851.

620

621 Freund TF & Antal M. (1988). GABA-containing neurons in the septum control inhibitory
622 interneurons in the hippocampus. *Nature* **336**, 170-173.

623

624 Friedel P, Kahle KT, Zhang J, Hertz N, Pisella LI, Buhler E, Schaller F, Duan J, Khanna AR,
625 Bishop PN, Shokat KM & Medina I. (2015). WNK1-regulated inhibitory phosphorylation of the
626 KCC2 cotransporter maintains the depolarizing action of GABA in immature neurons. *Sci*
627 *Signal* **8**, ra65.

628

629 Gan J, Weng SM, Pernia-Andrade AJ, Csicsvari J & Jonas P. (2017). Phase-Locked Inhibition,
630 but Not Excitation, Underlies Hippocampal Ripple Oscillations in Awake Mice In Vivo. *Neuron*
631 **93**, 308-314.

632

633 Gao B & Fritschy JM. (1994). Selective allocation of GABAA receptors containing the alpha 1
634 subunit to neurochemically distinct subpopulations of rat hippocampal interneurons. *The*
635 *European journal of neuroscience* **6**, 837-853.

636

637 Gauvain G, Chamma I, Chevy Q, Cabezas C, Irinopoulou T, Bodrug N, Carnaud M, Levi S &
638 Poncer JC. (2011). The neuronal K-Cl cotransporter KCC2 influences postsynaptic AMPA
639 receptor content and lateral diffusion in dendritic spines. *Proceedings of the National*
640 *Academy of Sciences of the United States of America* **108**, 15474-15479.

641

642 Gielen M, Thomas P & Smart TG. (2015). The desensitization gate of inhibitory Cys-loop
643 receptors. *Nature communications* **6**, 6829.

644

645 Goutierre M, Al Awabdh S, Donneger F, Francois E, Gomez-Dominguez D, Irinopoulou T,
646 Menendez de la Prida L & Poncer JC. (2019). KCC2 Regulates Neuronal Excitability and
647 Hippocampal Activity via Interaction with Task-3 Channels. *Cell reports* **28**, 91-103.e107.

648

649 Gulyas AI, Hajos N & Freund TF. (1996). Interneurons containing calretinin are specialized to
650 control other interneurons in the rat hippocampus. *The Journal of neuroscience : the official*
651 *journal of the Society for Neuroscience* **16**, 3397-3411.

652

653 Gulyas AI, Megias M, Emri Z & Freund TF. (1999). Total number and ratio of excitatory and
654 inhibitory synapses converging onto single interneurons of different types in the CA1 area of
655 the rat hippocampus. *The Journal of neuroscience : the official journal of the Society for*
656 *Neuroscience* **19**, 10082-10097.

657

658 Gulyas AI, Sik A, Payne JA, Kaila K & Freund TF. (2001). The KCl cotransporter, KCC2, is highly
659 expressed in the vicinity of excitatory synapses in the rat hippocampus. *The European*
660 *journal of neuroscience* **13**, 2205-2217.

661

662 Hartig W, Brauer K & Bruckner G. (1992). Wisteria floribunda agglutinin-labelled nets
663 surround parvalbumin-containing neurons. *Neuroreport* **3**, 869-872.

664

665 Henze DA & Buzsaki G. (2001). Action potential threshold of hippocampal pyramidal cells in
666 vivo is increased by recent spiking activity. *Neuroscience* **105**, 121-130.

667

668 Heubl M, Zhang J, Pressey JC, Al Awabdh S, Renner M, Gomez-Castro F, Moutkine I, Eugène
669 E, Rousseau M, Kahle KT, Poncer JC & Lévi S. (2017). GABAA receptor dependent synaptic
670 inhibition rapidly tunes KCC2 activity via the Cl⁻-sensitive WNK1 kinase. *Nature*
671 *communications* **8**, 1776.

672

673 Hu H, Gan J & Jonas P. (2014). Interneurons. Fast-spiking, parvalbumin(+) GABAergic
674 interneurons: from cellular design to microcircuit function. *Science* **345**, 1255-1263.

675

676 Huberfeld G, Wittner L, Clemenceau S, Baulac M, Kaila K, Miles R & Rivera C. (2007).
677 Perturbed chloride homeostasis and GABAergic signaling in human temporal lobe epilepsy.
678 *The Journal of neuroscience : the official journal of the Society for Neuroscience* **27**, 9866-
679 9873.

680

681 Ivakine EA, Acton BA, Mahadevan V, Ormond J, Tang M, Pressey JC, Huang MY, Ng D, Delpire
682 E, Salter MW, Woodin MA & McInnes RR. (2013). Neto2 is a KCC2 interacting protein
683 required for neuronal Cl⁻ regulation in hippocampal neurons. *Proceedings of the National
684 Academy of Sciences of the United States of America* **110**, 3561-3566.

685

686 Jedlicka P, Deller T, Gutkin BS & Backus KH. (2011). Activity-dependent intracellular chloride
687 accumulation and diffusion controls GABA(A) receptor-mediated synaptic transmission.
688 *Hippocampus* **21**, 885-898.

689

690 Jones MV & Westbrook GL. (1995). Desensitized states prolong GABAA channel responses to
691 brief agonist pulses. *Neuron* **15**, 181-191.

692

693 Jones MV & Westbrook GL. (1996). The impact of receptor desensitization on fast synaptic
694 transmission. *Trends in neurosciences* **19**, 96-101.

695

696 Kaila K, Lamsa K, Smirnov S, Taira T & Voipio J. (1997). Long-lasting GABA-mediated
697 depolarization evoked by high-frequency stimulation in pyramidal neurons of rat
698 hippocampal slice is attributable to a network-driven, bicarbonate-dependent K⁺ transient.
699 *The Journal of neuroscience : the official journal of the Society for Neuroscience* **17**, 7662-
700 7672.

701

702 Karlocai MR, Wittner L, Toth K, Magloczky Z, Katarova Z, Rasonyi G, Eross L, Czirjak S, Halasz
703 P, Szabo G, Payne JA, Kaila K & Freund TF. (2016). Enhanced expression of potassium-
704 chloride cotransporter KCC2 in human temporal lobe epilepsy. *Brain structure & function*
705 **221**, 3601-3615.

706

707 Kelley MR, Cardarelli RA, Smalley JL, Ollerhead TA, Andrew PM, Brandon NJ, Deeb TZ & Moss
708 SJ. (2018). Locally Reducing KCC2 Activity in the Hippocampus is Sufficient to Induce
709 Temporal Lobe Epilepsy. *EBioMedicine* **32**, 62-71.

710

711 Khirug S, Yamada J, Afzalov R, Voipio J, Khiroug L & Kaila K. (2008). GABAergic depolarization
712 of the axon initial segment in cortical principal neurons is caused by the Na-K-2Cl
713 cotransporter NKCC1. *The Journal of neuroscience : the official journal of the Society for*
714 *Neuroscience* **28**, 4635-4639.

715

716 Kim Y & Trussell LO. (2007). Ion channels generating complex spikes in cartwheel cells of the
717 dorsal cochlear nucleus. *Journal of neurophysiology* **97**, 1705-1725.

718

719 Kirmse K, Kummer M, Kovalchuk Y, Witte OW, Garaschuk O & Holthoff K. (2015). GABA
720 depolarizes immature neurons and inhibits network activity in the neonatal neocortex in
721 vivo. *Nature communications* **6**, 7750.

722

723 Klausberger T & Somogyi P. (2008). Neuronal diversity and temporal dynamics: the unity of
724 hippocampal circuit operations. *Science* **321**, 53-57.

725

726 Kourdougli N, Pellegrino C, Renko JM, Khirug S, Chazal G, Kukko-Lukjanov TK, Lauri SE,

727 Gaiarsa JL, Zhou L, Peret A, Castren EP, Tuominen RKP, Crepel V & Rivera CP. (2017).

728 Depolarizing GABA contributes to glutamatergic network rewiring in epilepsy. *Annals of*

729 *neurology* **81**, 251-265.

730

731 Le Roux N, Cabezas C, Bohm UL & Poncer JC. (2013). Input-specific learning rules at

732 excitatory synapses onto hippocampal parvalbumin-expressing interneurons. *The Journal of*

733 *physiology* **591**, 1809-1822.

734

735 Li H, Khirug S, Cai C, Ludwig A, Blaesse P, Kolikova J, Afzalov R, Coleman SK, Lauri S,

736 Airaksinen MS, Keinanen K, Khiroug L, Saarma M, Kaila K & Rivera C. (2007). KCC2 interacts

737 with the dendritic cytoskeleton to promote spine development. *Neuron* **56**, 1019-1033.

738

739 Llano I & Marty A. (1995). Presynaptic metabotropic glutamatergic regulation of inhibitory

740 synapses in rat cerebellar slices. *The Journal of physiology* **486 (Pt 1)**, 163-176.

741

742 Llano O, Smirnov S, Soni S, Golubtsov A, Guillemin I, Hotulainen P, Medina I, Nothwang HG,

743 Rivera C & Ludwig A. (2015). KCC2 regulates actin dynamics in dendritic spines via interaction

744 with beta-PIX. *The Journal of cell biology* **209**, 671-686.

745

746 Lozovaya N, Nardou R, Tyzio R, Chiesa M, Pons-Bennaceur A, Eftekhari S, Bui TT, Billon-Grand

747 M, Rasero J, Bonifazi P, Guimond D, Gaiarsa JL, Ferrari DC & Ben-Ari Y. (2019). Early

748 alterations in a mouse model of Rett syndrome: the GABA developmental shift is abolished
749 at birth. *Scientific reports* **9**, 9276.

750

751 MacKenzie G & Maguire J. (2015). Chronic stress shifts the GABA reversal potential in the
752 hippocampus and increases seizure susceptibility. *Epilepsy research* **109**, 13-27.

753

754 Magloire V, Cornford J, Lieb A, Kullmann DM & Pavlov I. (2019). KCC2 overexpression
755 prevents the paradoxical seizure-promoting action of somatic inhibition. *Nature*
756 *communications* **10**, 1225.

757

758 Mahadevan V, Pressey JC, Acton BA, Uvarov P, Huang MY, Chevrier J, Puchalski A, Li CM,
759 Ivakine EA, Airaksinen MS, Delpire E, McInnes RR & Woodin MA. (2014). Kainate receptors
760 coexist in a functional complex with KCC2 and regulate chloride homeostasis in hippocampal
761 neurons. *Cell reports* **7**, 1762-1770.

762

763 Markkanen M, Karhunen T, Llano O, Ludwig A, Rivera C, Uvarov P & Airaksinen MS. (2014).
764 Distribution of neuronal KCC2a and KCC2b isoforms in mouse CNS. *The Journal of*
765 *comparative neurology* **522**, 1897-1914.

766

767 Martina M, Royer S & Pare D. (2001). Cell-type-specific GABA responses and chloride
768 homeostasis in the cortex and amygdala. *Journal of neurophysiology* **86**, 2887-2895.

769

770 Marty A & Neher E. (1995). Tight-Seal Whole-Cell Recording. In *Single-Channel Recording*, ed.
771 Sakmann B & Neher E, pp. 31-52. Springer US, Boston, MA.

772

773 Mason MJ, Simpson AK, Mahaut-Smith MP & Robinson HP. (2005). The interpretation of
774 current-clamp recordings in the cell-attached patch-clamp configuration. *Biophysical journal*
775 **88**, 739-750.

776

777 Meijering E, Jacob M, Sarria JC, Steiner P, Hirling H & Unser M. (2004). Design and validation
778 of a tool for neurite tracing and analysis in fluorescence microscopy images. *Cytometry Part*
779 *A : the journal of the International Society for Analytical Cytology* **58**, 167-176.

780

781 Norenberg A, Hu H, Vida I, Bartos M & Jonas P. (2010). Distinct nonuniform cable properties
782 optimize rapid and efficient activation of fast-spiking GABAergic interneurons. *Proceedings*
783 *of the National Academy of Sciences of the United States of America* **107**, 894-899.

784

785 Palma E, Amici M, Sobrero F, Spinelli G, Di Angelantonio S, Ragozzino D, Mascia A, Scoppetta
786 C, Esposito V, Miledi R & Eusebi F. (2006). Anomalous levels of Cl⁻ transporters in the
787 hippocampal subiculum from temporal lobe epilepsy patients make GABA excitatory.
788 *Proceedings of the National Academy of Sciences of the United States of America* **103**, 8465-
789 8468.

790

791 Papke D, Gonzalez-Gutierrez G & Grosman C. (2011). Desensitization of neurotransmitter-
792 gated ion channels during high-frequency stimulation: a comparative study of Cys-loop,
793 AMPA and purinergic receptors. *The Journal of physiology* **589**, 1571-1585.

794

795 Patenaude C, Massicotte G & Lacaille JC. (2005). Cell-type specific GABA synaptic
796 transmission and activity-dependent plasticity in rat hippocampal stratum radiatum
797 interneurons. *The European journal of neuroscience* **22**, 179-188.

798

799 Perkins KL. (2006). Cell-attached voltage-clamp and current-clamp recording and stimulation
800 techniques in brain slices. *Journal of neuroscience methods* **154**, 1-18.

801

802 Pouille F & Scanziani M. (2001). Enforcement of temporal fidelity in pyramidal cells by
803 somatic feed-forward inhibition. *Science* **293**, 1159-1163.

804

805 Rivera C, Voipio J, Payne JA, Ruusuvuori E, Lahtinen H, Lamsa K, Pirvola U, Saarma M & Kaila
806 K. (1999). The K⁺/Cl⁻ co-transporter KCC2 renders GABA hyperpolarizing during neuronal
807 maturation. *Nature* **397**, 251-255.

808

809 Sauer JF & Bartos M. (2010). Recruitment of early postnatal parvalbumin-positive
810 hippocampal interneurons by GABAergic excitation. *The Journal of neuroscience : the official*
811 *journal of the Society for Neuroscience* **30**, 110-115.

812

813 Simat M, Ambrosetti L, Lardi-Studler B & Fritschy JM. (2007). GABAergic synaptogenesis
814 marks the onset of differentiation of basket and stellate cells in mouse cerebellum. *The*
815 *European journal of neuroscience* **26**, 2239-2256.

816

817 Solbach S & Celio MR. (1991). Ontogeny of the calcium binding protein parvalbumin in the
818 rat nervous system. *Anatomy and embryology* **184**, 103-124.

819

820 Staley KJ & Mody I. (1992). Shunting of excitatory input to dentate gyrus granule cells by a
821 depolarizing GABAA receptor-mediated postsynaptic conductance. *Journal of*
822 *neurophysiology* **68**, 197-212.

823

824 Staley KJ & Proctor WR. (1999). Modulation of mammalian dendritic GABA(A) receptor
825 function by the kinetics of Cl⁻ and HCO₃⁻ transport. *The Journal of physiology* **519 Pt 3**, 693-
826 712.

827

828 Takacs VT, Klausberger T, Somogyi P, Freund TF & Gulyas AI. (2012). Extrinsic and local
829 glutamatergic inputs of the rat hippocampal CA1 area differentially innervate pyramidal cells
830 and interneurons. *Hippocampus* **22**, 1379-1391.

831

832 Tang X, Kim J, Zhou L, Wengert E, Zhang L, Wu Z, Carromeu C, Muotri AR, Marchetto MC,
833 Gage FH & Chen G. (2016). KCC2 rescues functional deficits in human neurons derived from
834 patients with Rett syndrome. *Proceedings of the National Academy of Sciences of the United*
835 *States of America* **113**, 751-756.

836

837 Thompson SM & Gahwiler BH. (1989a). Activity-dependent disinhibition. I. Repetitive
838 stimulation reduces IPSP driving force and conductance in the hippocampus in vitro. *Journal*
839 *of neurophysiology* **61**, 501-511.

840

841 Thompson SM & Gahwiler BH. (1989b). Activity-dependent disinhibition. II. Effects of
842 extracellular potassium, furosemide, and membrane potential on ECl⁻ in hippocampal CA3
843 neurons. *Journal of neurophysiology* **61**, 512-523.

844

845 Thompson SM & Gahwiler BH. (1989c). Activity-dependent disinhibition. III. Desensitization
846 and GABAB receptor-mediated presynaptic inhibition in the hippocampus in vitro. *Journal of*
847 *neurophysiology* **61**, 524-533.

848

849 Tyzio R, Nardou R, Ferrari DC, Tsintsadze T, Shahrokhi A, Eftekhari S, Khalilov I, Tsintsadze V,
850 Brouchoud C, Chazal G, Lemonnier E, Lozovaya N, Burnashev N & Ben-Ari Y. (2014).
851 Oxytocin-mediated GABA inhibition during delivery attenuates autism pathogenesis in
852 rodent offspring. *Science* **343**, 675-679.

853

854 Uvarov P, Ludwig A, Markkanen M, Pruunsild P, Kaila K, Delpire E, Timmusk T, Rivera C &
855 Airaksinen MS. (2007). A novel N-terminal isoform of the neuron-specific K-Cl cotransporter
856 KCC2. *The Journal of biological chemistry* **282**, 30570-30576.

857

858 Verheugen JA, Fricker D & Miles R. (1999). Noninvasive measurements of the membrane
859 potential and GABAergic action in hippocampal interneurons. *The Journal of neuroscience :*
860 *the official journal of the Society for Neuroscience* **19**, 2546-2555.

861

862 Zucker RS & Regehr WG. (2002). Short-term synaptic plasticity. *Annu Rev Physiol* **64**, 355-
863 405.

864

865

866

867 **Acknowledgements**

868 We thank X. Marques for expert assistance with confocal imaging, which was performed at
869 the “Photonic Imaging and Image Analysis Platform” of the Institut du Fer à Moulin. We also
870 thank Peter Blaesse for critical reading of the manuscript.

871

872 **Competing interests**

873 The authors declare no conflict of interest.

874

875

876 **Author contributions**

877 Y.O. and J.C.P. conceived and designed the research. Y.O. performed all electrophysiological
878 recordings and data analysis with help of E.J.S. who also maintained the mouse colony. F.D.
879 performed immunohistochemistry, confocal imaging and analysis. Y.O and J.C.P. prepared the
880 figures and wrote the paper. All authors approved the final version of the manuscript and
881 agree to be accountable for all aspects of the work in ensuring that questions related to the
882 accuracy or integrity of any part of the work are appropriately investigated and resolved. All
883 persons designated as authors qualify for authorship, and all those who qualify for authorship
884 are listed.

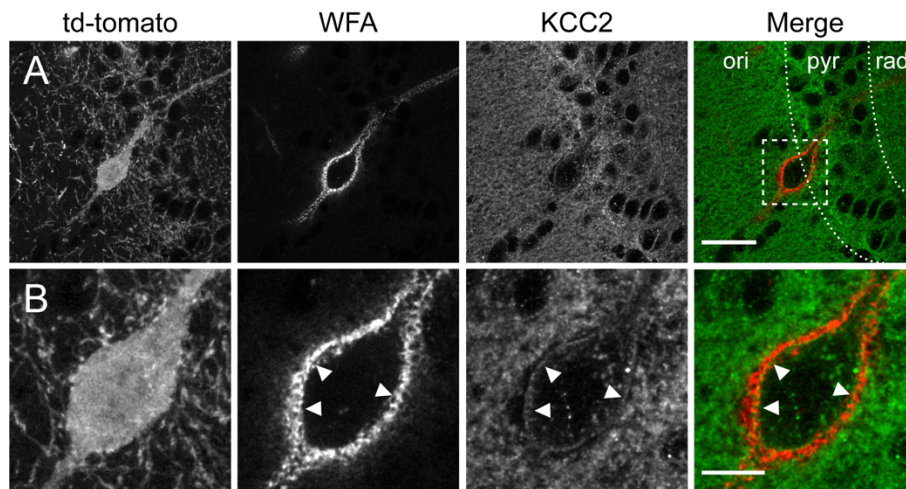
885

886

887 **Funding**

888 This work was supported by the Institut National de la Santé et de la Recherche Médicale,
889 Sorbonne Université, LabEx Bio-Psy through the *Investissements d'Avenir* program managed
890 by Agence Nationale de La Recherche under reference ANR-11-IDEX-0004-02 (postdoctoral
891 fellowship to YO), Fondation pour la Recherche Médicale (grant DEQ20140329539 to JCP),
892 Fédération pour la Recherche sur le Cerveau and Fondation Française pour la Recherche sur
893 l'Épilepsie (grants to JCP) as well as ERANET-Neuron (ACRoBAT project, funded by Agence
894 Nationale pour la Recherche to JCP). FD is the recipient of a doctoral fellowship from Sorbonne
895 Université. The Poncer lab is affiliated with the Paris School of Neuroscience (ENP) and the
896 Bio-Psy Laboratory of excellence.

897

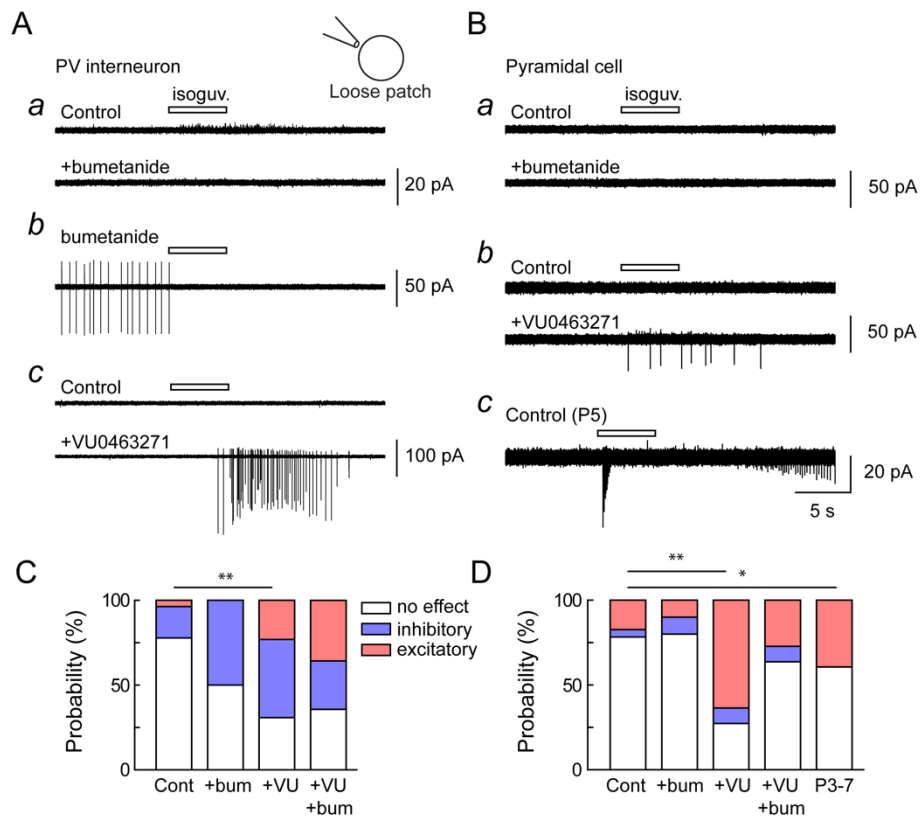


899

900 **Figure 1. KCC2 labeling of hippocampal CA1 parvalbumin interneurons.**

901 A, Representative micrograph (maximum projection of 10 confocal sections over 2.6 μm) of
 902 area CA1 of an adult *Pvalb^{tm1(cre)Arbr/J}::Ai14* mouse hippocampal section immunostained for
 903 KCC2 (green) and WFA lectin (red), showing td-tomato expression in a PV IN surrounded by
 904 WFA staining on the soma and proximal dendrites. Right, merged images of KCC2 and WFA
 905 stainings. Scale, 30 μm . B, Magnified region boxed in A, showing KCC2 immunostaining in td-
 906 tomato expressing PV IN lies just underneath the perineuronal net stained with WFA
 907 (arrowheads). Scale, 10 μm .

908

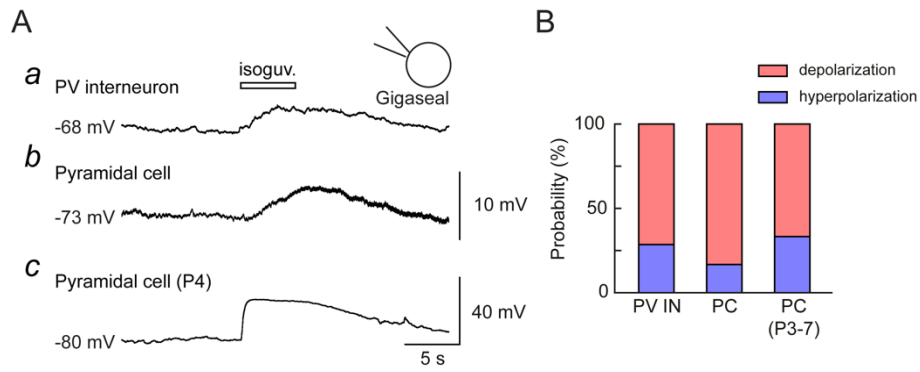


909

910 **Figure 2. Excitatory and inhibitory actions of GABAA receptor activation in CA1 parvalbumin**
 911 **interneurons and pyramidal cells.**

912 *A a*, Representative sections of recordings in loose patch mode of a CA1 PV IN upon brief, focal
 913 somatic application of isoguvacine (100 μ M, white bar), before and during application of the
 914 NKCC1 antagonist bumetanide (10 μ M). *b*, same as in *a* in another PV IN during bumetanide
 915 application. *c*, same as in *a* and *b*, before and during application of the KCC2 antagonist
 916 VU0463271 (10 μ M). *B a* and *b*, recordings as in *A a* and *c* from CA1 PCs in P30-P40 mice. *c*,
 917 recording showing the effect of somatic isoguvacine application on a CA1 PC from a P5 mouse.
 918 *C*, summary graph showing the proportions of each type response (excitatory, inhibitory or
 919 none) recorded upon isoguvacine application in PV INs. *D*, Same as *C* for recordings from PCs.
 920 χ^2 test * $p < 0.05$, ** $p < 0.02$.

921

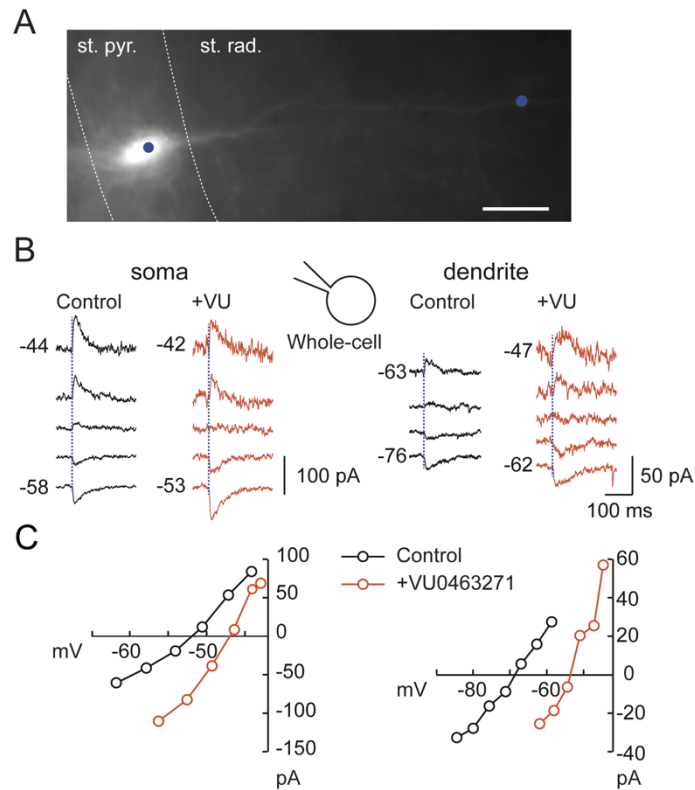


922

923 **Figure 3. Polarity of GABAAR-mediated potentials in CA1 parvalbumin interneurons and**
 924 **pyramidal cells.**

925 A, Representative sections of recordings in gigaseal patch mode of a CA1 PV IN from a P46
 926 mouse (*a*) and a PC from a P33 (*b*) or P4 (*c*) mouse upon brief, focal somatic application of
 927 isoguvacine (100 μ M, white bar). B, summary graph showing the proportions of each type of
 928 response (depolarizing, hyperpolarizing) recorded upon isoguvacine application in each cell
 929 type.

930

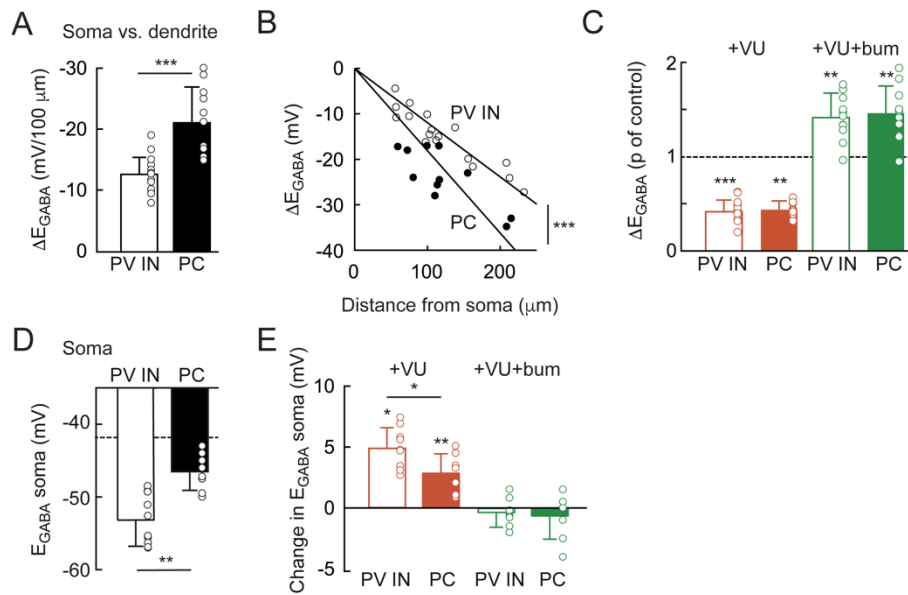


931

932 **Figure 4. Contribution of KCC2 to transmembrane chloride extrusion in a CA1 parvalbumin**
 933 **interneuron.**

934 A, Fluorescence micrograph of a CA1 PV IN from a P37 mouse hippocampal slice, recorded in
 935 whole-cell mode and filled with Alex594. The blue spots represent the position and size of the
 936 laser beam used for focal RubiGABA photolysis. Scale, 20 μm . B, Currents evoked at varying
 937 potentials by focal somatic (left) or dendritic (right) photolysis of RubiGABA in the cell shown
 938 in A, before (black) and during (red) application of VU0463271 (10 μM). Numbers of the right
 939 represent holding potentials corrected for liquid junction potential and voltage drop across
 940 the pipette resistance. C, Current-voltage relations from recordings shown in B showing the
 941 different reversal potentials of RubiGABA-evoked currents in the soma vs. dendrites and their
 942 depolarizing shift upon KCC2 blockade.

943



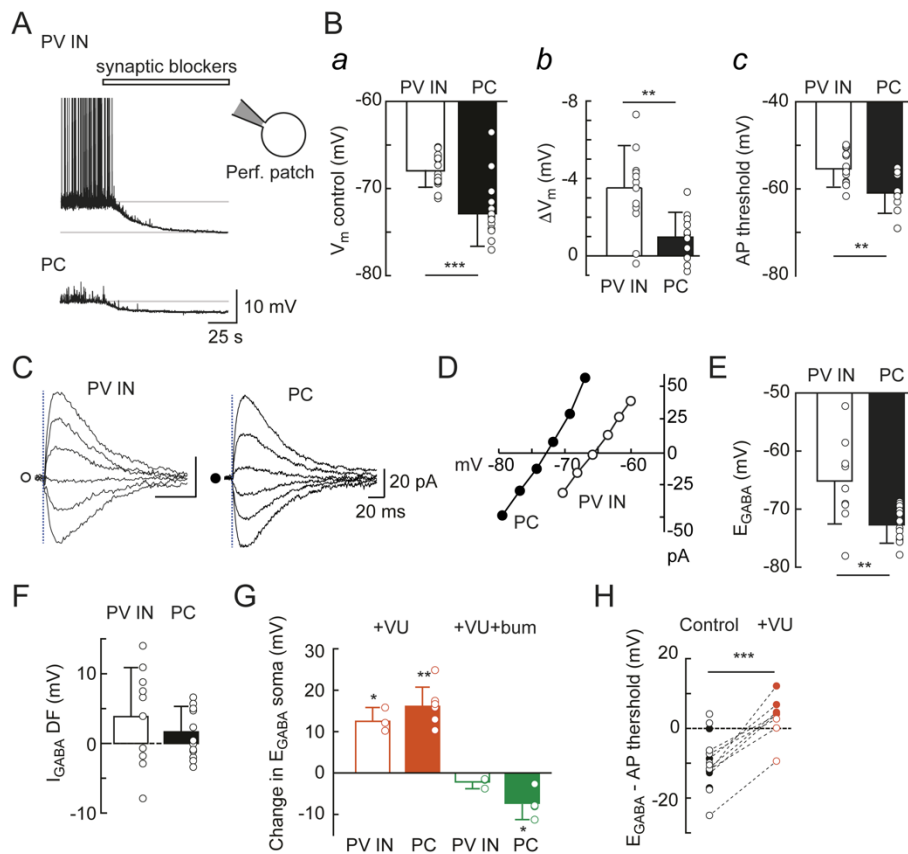
944

945 **Figure 5. Compared contribution of KCC2 and NKCC1 to somato-dendritic chloride gradients**
 946 **in CA1 parvalbumin interneuron and pyramidal cells.**

947 A, Summary graph showing E_{GABA} somatodendritic gradient (ΔE_{GABA}) between soma and
 948 dendrites normalized by the distance from soma to dendritic photolysis locations. PV IN: n=17
 949 dendritic sites in 9 cells. PC: n=11 dendritic sites in 8 cells. *** Mann Whitney test $p < 0.001$. B,
 950 somatodendritic E_{GABA} gradient plotted against the distance from soma to dendritic photolysis
 951 locations with superimposed linear regression, showing steeper relation in PCs compared with
 952 PV INs. Same data as in A, *** Multiple regression test $p < 0.001$. C, Change in ΔE_{GABA} upon
 953 sequential KCC2 (red) and KCC2+NKCC1 blockade (green) by VU0463271 and bumetanide,
 954 respectively. The values are normalized to those of the preceding condition (control for
 955 VU0463271, VU0463271 for VU0463271+bumetanide). ** and *** Wilcoxon signed-rank test
 956 $p < 0.01$ and 0.001 , respectively. No significant difference was observed in PC vs PV INs. Same
 957 recordings as in A and B. D, Reversal potential (E_{GABA}) of currents evoked by somatic RubiGABA
 958 uncaging in PV INs and PCs. Same data as in A-C. Dashed line: estimated E_{Cl} based on Nernst
 959 equation. ** Mann Whitney test $p < 0.01$. E, Change in somatic E_{GABA} upon sequential KCC2

960 (red) and KCC2+NKCC1 blockade (green) by VU0463271 and bumetanide, respectively. The
961 values are normalized to those of the preceding condition (control for VU0463271,
962 VU0463271 for VU0463271+bumetanide). VU0463271 depolarized E_{GABA} more in PV INs than
963 in PCs. However, further addition of bumetanide had no significant effect. * and ** Wilcoxon
964 rank signed-rank test $p < 0.05$ and 0.01 , respectively. * for PV INs vs PCs, Mann Whitney test
965 $p < 0.05$.

966



967

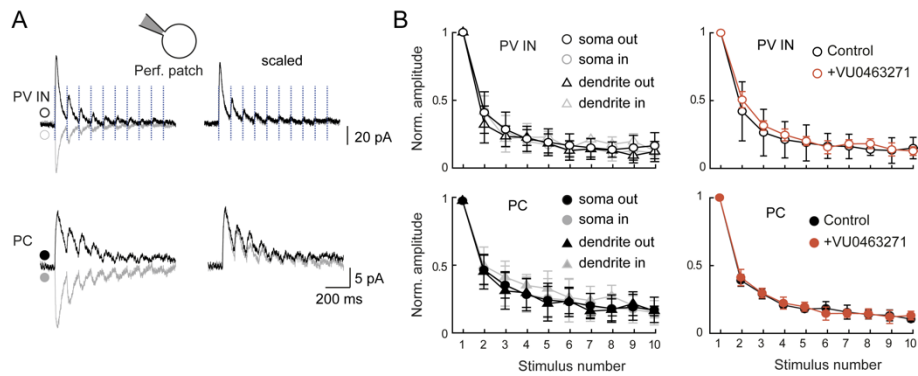
968 **Figure 6. Compared reversal potential and driving force of GABA currents in CA1**
 969 **parvalbumin interneurons and pyramidal cells.**

970 A, Representative current clamp recordings from a CA1 PV IN (top) and PC (bottom) in
 971 gramicidin-perforated patch mode, showing the effect of synaptic receptor antagonists (APV,
 972 NBQX and CGP55845) and TTX (white bar) on holding potential. Note that the PV IN but not
 973 the PC shows spontaneous firing prior to application of the blockers. B, *a*, resting membrane
 974 potential measured in 15 CA1 PV INs and 15 PCs prior to application of synaptic blockers. ***,
 975 Mann Whitney test $p < 0.001$. *b*, change in membrane potential (ΔV_m) upon application of
 976 synaptic blockers in the same cells as in *a*. **, Mann Whitney test $p < 0.01$. *c*, Action potential
 977 threshold measured in spontaneously firing PV INs ($n=15$) and PCs ($n=9$). **, Mann Whitney
 978 test $p < 0.01$. C, Currents evoked at varying potentials by focal somatic photolysis of RubiGABA
 979 in a PV IN (left) and a PC (right). The dotted line represents the timing of photolysis. D,

980 corresponding current/voltage relation for the recordings shown in C. Open circles, PV IN.
981 Filled circles, PC. E, Summary graphs showing the reversal potential of somatically evoked
982 GABAAR-mediated currents in 10 CA1 PV INs and 16 PCs. **, Mann Whitney test $p < 0.01$. F,
983 estimated driving force of somatic GABAAR-mediated currents computed by subtracting V_m
984 from E_{GABA} , showing GABAARs have slightly depolarizing actions in both PV INs and PCs. G,
985 summary graph showing the change in somatic E_{GABA} upon sequential KCC2 (red) and
986 KCC2+NKCC1 blockade (green) by VU0463271 and bumetanide, respectively. The values are
987 normalized to those of the preceding condition (control for VU0463271, VU0463271 for
988 VU0463271+bumetanide). Addition of bumetanide after VU0463271 had no significant effect
989 on somatic E_{GABA} in either PV INs (n=3) or PCs (n=4). *, paired t-test, $p < 0.05$; **, Wilcoxon
990 signed rank test, $p < 0.01$. H, Difference between E_{GABA} and firing threshold for PV INs (open
991 circles) and PCs (filled circles), before (black) and during (red) application of VU0463271.
992 Dotted lines represent paired data used for statistical comparison (all cells pooled). ***, Paired
993 t-test, $p < 0.001$.

994

995



996

997 **Figure 7. Dynamics of GABAAR-mediated currents in CA1 parvalbumin interneurons and**
 998 **pyramidal cells.**

999 A, Representative recordings of currents evoked by 10 Hz somatic photolysis of RubiGABA in
 1000 a CA1 PV IN and a PC recorded in gramicidin-perforated patch mode and held at potentials
 1001 above (black) or below (grey) E_{GABA} (PV IN: -60 and -80 mV; PC: -60 and -77 mV). B, Summary
 1002 graphs showing peak current amplitudes normalized to the peak amplitude of the first current,
 1003 during a train of RubiGABA photolysis on the soma (circles) or dendrites (triangles) of PV INs
 1004 (soma: n=6, dendrites: n=3, open symbols) and PCs (soma: n=11, dendrites: n=4, filled
 1005 symbols). C, Same as in B showing the lack of effect of VU0463271 (10 μ M, red symbols) on
 1006 the decay of the peak amplitude of GABAAR-mediated currents during a 10 Hz somatic
 1007 RubiGABA photolysis (PV INs, n=2; PCs, n=4).